Self-association of TPR domains : lessons learned from a designed, consensus-based TPR oligomer

Krachler, Anne-Marie; Sharma, Amit; Kleanthous, Colin

DOI:
10.1002/prot.22726

Document Version
Publisher final version (usually the publisher pdf)

Citation for published version (Harvard):
Krachler, A-M, Sharma, A & Kleanthous, C 2010, 'Self-association of TPR domains : lessons learned from a designed, consensus-based TPR oligomer' Proteins: structure, function, and bioinformatics, vol 78, no. 9, pp. 2131-2143., 10.1002/prot.22726

PROTEINS
STRUCTURE ■ FUNCTION ■ BIOINFORMATICS

Self-association of TPR domains: Lessons learned from a designed, consensus-based TPR oligomer

Anne Marie Krachler, Amit Sharma, and Colin Kleanthous*

Department of Biology, University of York, Heslington, York YO10 5YW, United Kingdom

ABSTRACT

The tetratricopeptide repeat (TPR) motif is a protein–protein interaction module that acts as an organizing centre for complexes regulating a multitude of biological processes. Despite accumulating evidence for the formation of TPR oligomers as an additional level of regulation there is a lack of structural and solution data explaining TPR self-association. In the present work we characterize the trimeric TPR-containing protein YbgF, which is linked to the Tol system in Gram-negative bacteria. By subtracting previously identified TPR consensus residues required for stability of the fold from residues conserved across YbgF homologs, we identified residues involved in oligomerization of the C-terminal YbgF TPR domain. Crafting these residues, which are located in loop regions between TPR motifs, onto the monomeric consensus TPR protein CTPR3 induced the formation of oligomers. The crystal structure of this engineered oligomer shows an asymmetric trimer where stacking interactions between the introduced tyrosines and displacement of the C-terminal hydrophilic capping helix, present in most TPR domains, are key to oligomerization. Asymmetric trimerization of the YbgF TPR domain and CTPR3Y3 leads to the formation of higher order oligomers both in the crystal and in solution. However, such open-ended self-association does not occur in full-length YbgF suggesting that the protein's N-terminal coiled-coil domain restricts further oligomerization. This interpretation is borne out in experiments where the coiled-coil domain of YbgF was engineered onto the N-terminus of CTPR3Y3 and shown to block self-association beyond trimerization. Our study lays the foundations for understanding the structural basis for TPR domain self-association and how such self-association can be regulated in TPR domain-containing proteins.

Proteins 2010; 78:2131–2143.

Key words: protein engineering; tetratricopeptide repeat; self-association; oligomerization; protein–protein interaction.

INTRODUCTION

During the course of evolution a wealth of protein domains specialized in mediating protein–protein interactions have arisen which are often fused to other, functionally active parts of proteins to allow their integration into regulatory networks. The tetratricopeptide repeat (TPR) motif is a well studied example of a module facilitating protein–protein interactions. It was first discovered in yeast cell cycle regulatory proteins[1,2] but has since been identified in all kingdoms of life and a wide range of cellular compartments and has been associated with cellular processes as diverse as transcriptional regulation, mRNA processing and protein folding and translocation.[3]

TPR motifs consist of 34 amino acids which despite their loosely conserved sequence always assemble into a characteristic helix-turn-helix structure. Eight positions within the motif show a high propensity for certain types of amino acids: Large hydrophobic residues are preferred at positions 4, 7, 11 and 24, while positions 8, 20 and 27 are more frequently occupied by small hydrophobic residues. This patterning enables helix-helix packing within the motif and guarantees the structural integrity of the fold. Position 32 is often a proline which terminates the second helix (αB) in the motif.[4] Most TPR domains contain multiple motifs arrayed in tandem thereby forming an extended, right-handed superhelical arrangement, and are terminated by a C-terminal hydrophilic "capping-helix" that is thought to enhance solubility.[5–7] Ligand-binding predominantly takes place on the concave surface of TPR domains,[8–11] although examples are known where larger ligands make contact with both the concave and convex side of the helical array, as observed in the

Abbreviations: CTPR3, three-repeat consensus TPR protein; CTPR3Y3, CTPR3 Asp39Tyr Asp73Tyr Asp107Tyr; DSP, dithiobis(succinimidyl propionate); HMM, Hidden Markov Model; SEC-MALLS, size exclusion multiangle laser light scattering; TPR, tetratricopeptide repeat.

Anne Marie Krachler's current address is Department of Molecular Biology, UT Southwestern Medical Centre, 5323 Harry Hines MC:9148, TX 75390, USA
Amit Sharma's current address is Department of Biophysics, Johns Hopkins University, 3400 North Charles Street, Baltimore MD 21218, USA
Grant sponsor: European Union framework programme 6 (Research Training Network ProSA), BBSRC.
*Correspondence to: Colin Kleanthous, Department of Biology, University of York, Heslington, PO Box 373, York YO10 5YW, UK. E-mail: ck11@york.ac.uk
Received 11 January 2010; Revised 10 March 2010; Accepted 17 March 2010
Published online 23 March 2010 in Wiley InterScience (www.interscience.wiley.com).
DOI: 10.1002/prot.22726

crystal structure of the Fis1/Caf4 complex.[12] Most studies to date have focused on heterocomplexes formed between TPR domains and their non-TPR ligands. However, more recently it has become apparent that some TPR proteins not only bind heterologous ligands but can also self-assemble into higher order structures, either intrinsically or in response to external stimuli.[13–19] This additional level of regulation allows for the fine-tuning of biological processes and its absence can be deleterious even if binding of the heteroligand remains undisturbed. For example, the TPR-containing protein rapsyn, which is found at the neuromuscular synapse, plays an essential role in synaptic development and its ability to form higher order oligomers which recruit and cluster acetylcholine receptors at the neuromuscular junction depends on the presence of its TPR-domains.[13,14] The mitochondrial outer membrane protein Fis1 is involved in mitochondrial fission, the absence of which leads to pathological deformations in mitochondria. Its two TPR motifs have been shown to be involved in recruitment of the scission protein DLP1 to the membrane as well as self-association, with both processes being essential for the fission process.[16] Although these examples highlight the biological importance of TPR-mediated oligomerization in most cases it remains unclear if the contacts formed between TPR subunits are similar or distinct to those seen in heterocomplex formation. In the few cases where structures of TPR dimers or tetramers have been solved, solution data to confirm the biological relevance of oligomeric states and interfaces observed in the crystal are often absent or contradictory.

In this work, we identify key residues involved in oligomerization of YbgF, a previously uncharacterized oligomeric TPR protein from *E. coli*, and validate their involvement in TPR self-association by solution methods. By analyzing 3418 TPR-containing proteins, Main *et al.*[4,5] identified the amino acid with the highest propensity for each of the 34 positions within the motif, thereby creating a TPR consensus sequence. Proteins consisting of up to 20 such consensus TPR motifs in tandem (CTPRs) were constructed and were shown to be more stable than equivalent natural TPR domains and to be devoid of any ligand binding specificity.[4,20,21] In an attempt to design an oligomeric TPR domain we engineered residues we identified as relevant for the self-association of the YbgF TPR oligomer into a three-repeat version of the consensus TPR protein (CTPR3,[5]), which we show causes the previously monomeric protein to form oligomers in solution. We also report the structure of this engineered TPR domain from which we elucidate important principles for the formation of higher order TPR-oligomers that will likely underpin self-association in other TPR-containing proteins.

MATERIALS AND METHODS

Expression constructs

Full-length YbgF (excluding res. 1–26 which constitute a signal peptide), YbgF NTD (YbgF res. 27–109) and YbgF TPR domain (YbgF res. 139–263) were amplified from *E. coli* MG1566 genomic DNA using primers YbgFfw (5′-CAGT*CCATGG*GGATGCAGGCACCAATCAG TAGT-3′) and YbgFrev (5′-CAGT*CTCGAG*TTACATCGCG TTCAGACGTT-3′), NTDfw (5′-CAGT*CCATGG*CATCAG GCTCGGTCGAA-3′) and NTDrev (5′-CAGT*CTCGAG*T TATTGCGCCGCTGCAC-3′) or TPRfw (5′-CAGT*CCATGG* GGAGCGGTAATGCAAACAC-3′) and YbgFrev and cloned into NcoI/XhoI sites of pET21d (restriction sites underlined). The YbgF NTD-CTPR3Y3 fusion was generated by SOE PCR. YbgF NTD and CTPR3Y3 domains were initially amplified using primers YbgFfw and NTDs1 (5′-AGGTTGTACCATGCCTCAGCTGCATTACCGCTTTT CACC-3′) and CTPR3Y3fw (5′-GGTGAAAAGCGGTAA TGCAGCTGAGGCATGGTACAACCT-3′) and CTPR3Y3rev (5′CAGT*AAGCTT*TCAACCCTGTTTCTGTTTAGCG-3′), respectively. A second round of PCR was performed using the resulting products as template and primers YbgFfw and CTPR3Y3rev. The final PCR product was cloned into the NcoI/HindIII sites of pET21d. CTPR3ΔC was amplified using primers CTPRfw (5′-CAGT*GGATCC* GGGTAACTCCGCTGAGGC-3′) and CTPRrev (5′-CAGT *AAGCTT*CTAGTTGTTCGGGTCCAGTTC-3′), with pProEX HTa containing CTPR3 as template and cloned into BamHI/HindIII sites of the same plasmid. Site-directed YbgF TPR mutants were constructed by quick-change mutagenesis as were the double mutant CTPR3 D39Y D73Y and CTPR3Y3 (CTPR3 D39Y D73Y D107Y).

Protein expression and purification

YbgF, NTD, TPR domains and the YbgF NTD-CTPR3Y3 fusion were purified from BL21(DE3) cells after induction with 0.8 m*M* IPTG at 37°C for 4 h. Cells resuspended in 50 m*M* Tris pH 8.0 containing 5 m*M* $MgCl_2$, 10 m*M* PMSF and 2 mg/mL lysozyme were lysed by sonication. Cleared lysates were subjected to ammonium sulphate fractionation, with all proteins precipitating at 50% saturation. Proteins were re-solubilized in 50 m*M* Tris pH 8.0, loaded onto an SP Sepharose column (GE Healthcare) and eluted using a sodium chloride gradient (elution at a concentration of 200–300 m*M* NaCl). Final purification was accomplished using a Superdex S75 HL26/60 size exclusion column (Amersham) equilibrated with 50 m*M* Tris pH 7.5, 250 m*M* NaCl. CTPR3, CTPR3Y3, and CTPR3ΔC were expressed and purified as described previously.[5] The purity of all proteins was >95% as determined by SDS-PAGE and their masses were verified using ESI-MS (Waters LCT Premier XE mass spectrometer).

Circular dichroism experiments

For CD experiments, proteins were prepared in 10 m*M* sodium phosphate buffer pH 7.0 at concentrations between 5 and 15 μ*M*. Spectra were recorded at 20°C on

a Jasco J810 CD spectrophotometer using 1-mm path length quartz cuvettes. Scans were performed from 260 to 190 nm with a scanning rate of 100 nm/min, a data pitch of 1 nm and a multiplicity of 5. For thermal denaturation experiments, data were collected in 5°C increments over a temperature range of 20–90°C with an equilibration phase of 1 min at each temperature and a heating rate of 0.5°C/min. The reversibility of unfolding was between 95 and 98% for all analyzed proteins. Spectra were analyzed for secondary structure content using the software CDNN.[22]

Chemical crosslinking

Protein samples were prepared at concentrations between 0.5 and 100 μ*M* in 10 m*M* sodium phosphate buffer pH 7.0 and a 10-fold molar excess of the crosslinker dithiobis (succinimidyl propionate) (DSP, Pierce) was added. Reactions were left to proceed at room temperature for 30 min and finally quenched by adding a 100-fold molar excess of Tris pH 8.0. Samples were analyzed by nonreducing SDS-PAGE to preserve the crosslinks or reduced by adding 20 m*M* DTT prior to gel loading in case of the control.

Size exclusion chromatography and multiangle light scattering

Proteins for SEC-MALLS were typically prepared at concentrations ranging from 10 to 200 μ*M* in 20 m*M* Tris pH 7.5, 150 m*M* NaCl. For the chromatographic step, a Superdex™ 75 HR 10/300 GL column (Amersham) was used at a flow rate of 0.5 mL/min. A Wyatt Dawn Heleos-II multiangle laser light scattering instrument and an Optilab Rex Refractive index detector were used at 25°C for data collection, molecular weights were calculated using the Astra software (Wyatt).

Analytical ultracentrifugation

Sedimentation velocity experiments were carried out in a Beckman Optima XL/I analytical ultracentrifuge, using 12-mm path length cells in an AN-60Ti rotor. YbgF was prepared at concentrations of 50, 25, and 12.5 μ*M* in 100 m*M* phosphate buffer pH 7.5. Experiments were run at 20°C and a speed of 45,000 rpm Protein sedimentation was followed by absorbance at 235 nm every minute over the course of the experiment (90 min). Data were analyzed using SEDFIT software.[23]

Crystallization of CTPR3Y3

Purified protein was set up as sitting drops in Hampton screens 1 + 2, Index and PACT screens (Hampton Research) at a concentration of 20 mg/mL in 10 m*M* Tris pH 7.5. The best crystals were obtained in 0.1*M* malic acid, MES, Tris pH 4.0, 25% PEG1500 at 20°C overnight. Crystals used for data collection were obtained under identical conditions but after the addition of 5% ethylene glycol as additive, at a protein concentration of 10 mg/mL in 2 μL hanging drops after three days.

Data collection and refinement

Diffraction data for the CTPR3Y3 crystals were collected at the European Synchrotron Radiation Facility (ESRF), beam line ID14-1. Data were collected at a wavelength of 0.9334 Å over a range of 120° with an oscillation of 0.5°. HKL-2000 was used for data integration and scaling.[24] Reflections were indexed in space group $P6_522$ with unit cell dimensions of $a = b = 62.3$ and $c = 120.4$ Å. The crystal structure of CTPR2 (1na3.pdb) with a sequence identity of 97% was used as the search model. The program MRBUMP from the CCP4 (Collaborative Computational Project No.4) suite was used to generate a solution after molecular replacement. Iterative rounds of model building using COOT and restrained refinement using REFMAC5[25,26] were carried out before water molecules were built using ARP/wARP_solvent. The final model was validated using MOLPROBITY.[27] Data collection and refinement statistics are presented in Table I. Analysis of the 1.86 Å resolution dataset using CTRUNCATE from the CCP4i suite of programs indicated extreme anisotropy, with eigen values being 0.9190: 0.9190: 1.1620, and little observable diffraction beyond 2.8 Å in the c^* axis. This, in addition to the high redundancy of the data, distorts the isotropically tabulated statistics leading to exaggerated Rmerge values. However, inclusion of high resolution data substantially improved the density maps, with the maximum likelihood weighting scheme lowering the contribution from weakly observed reflections during refinement.

Accession numbers

Coordinates and structure factors for CTPR3Y3 have been deposited in the Protein Data Bank with accession number 2WQH.

RESULTS

Trimerization of YbgF and its individual domains

TPRs are prevalent in all kingdoms of life—36 TPR domain containing proteins have been annotated in the *Escherichia coli* genome alone.[28] We purified and characterized the periplasmic TPR-containing protein YbgF from *E. coli*, a 25 kDa protein which has been shown to interact with TolA, a member of the Tol protein complex involved in outer membrane maintenance and uptake of filamentous phages and bacteriocins in Gram-negative bacteria.[29–32] Analytical ultracentrifugation and size-exclusion chromatography-multiangle light scattering

Table I
Data Collection and Refinement Statistics for CTPR3Y3

Data collection	
Wavelength (Å)	0.9334
Space group	$P6_522$
Cell dimensions	
a/*b*/*c* (Å)	62.28/62.28/120.37
α/β/γ (°)	90/90/120
Resolution (Å)[a]	50.0–2.21 (2.29–2.21)
R_{merge}[a,b]	0.20 (0.66)
$I/\sigma(I)$[a]	11.61 (4.54)
Total number of reflections	1,061,821
Number of unique reflections	13,174
Completeness (%)[a]	99.1 (98.8)
Redundancy[a]	8.3 (7.4)
Refinement	
Resolution (Å)[a]	49.22–2.20
Number of reflections	7519
R_{work}/R_{free}[c]	23.5/28.5
Number of atoms	
Protein	901
Water	10
MPD	16
Ethylene glycol	8
B-factors (Å^2)	
Protein	36.11
Water	36.53
MPD	83.91
Ethylene glycol	59.23
Rmsd[d]	
Bonds (Å)	0.01
Angles (°)	1.18
Ramachandran plot	
Favored region (%)	98
Allowed region (%)	2
Disallowed region (%)	0

[a]Limits and values for the outer resolution bin are given in parentheses.
[b]$R_{merge} = \Sigma\Sigma|I_{i,j} - \langle I_j \rangle|/\Sigma\Sigma I_{i,j}$
[c]$R = \Sigma_{hkl}|F_{hkl}^{obs} - F_{hkl}^{calc}|/\Sigma_{hkl} F_{hkl}^{obs}$
[d]Root-mean-square deviation given from ideal values.

(SEC-MALLS) of intact YbgF all showed that the protein forms a stable trimer in solution (see Fig. 1). Two domains—an N-terminal coiled-coil and a C-terminal TPR domain containing three consecutive repeats—were identified in YbgF by sequence analysis. Following expression and purification of the N-terminal coiled-coil (NTD, 9 kDa) and C-terminal TPR domains (14 kDa), chemical cross-linking was used to investigate self-association of these individual domains relative to YbgF. Dimeric and trimeric species could be seen for all proteins the only difference between them being the presence of higher order oligomeric species in the TPR domain construct [Fig. 1(c)]. As such higher order oligomers were not observed in intact YbgF cross-linking reactions (nor in AUC or SEC-MALLS experiments) this implies that the trimeric NTD limits the propensity of the YbgF TPR domain to self-associate into oligomers greater than trimers, a point we return to below.

Conserved residues that deviate from the TPR consensus sequence are key to oligomerization

Residues which are conserved within a class of homologous TPR-domains but deviate from the consensus sequence are often functionally important.[33] We applied this principle to YbgF to identify residues which could potentially be involved in oligomerization of its TPR domain. YbgF is well conserved in most Gram-negative bacteria and so we used 40 YbgF homologs from Proteobacteria to generate a multiple sequence alignment and HMM logo for each of the three TPR motifs.[34–36] Comparison of the three TPR HMM logos with the

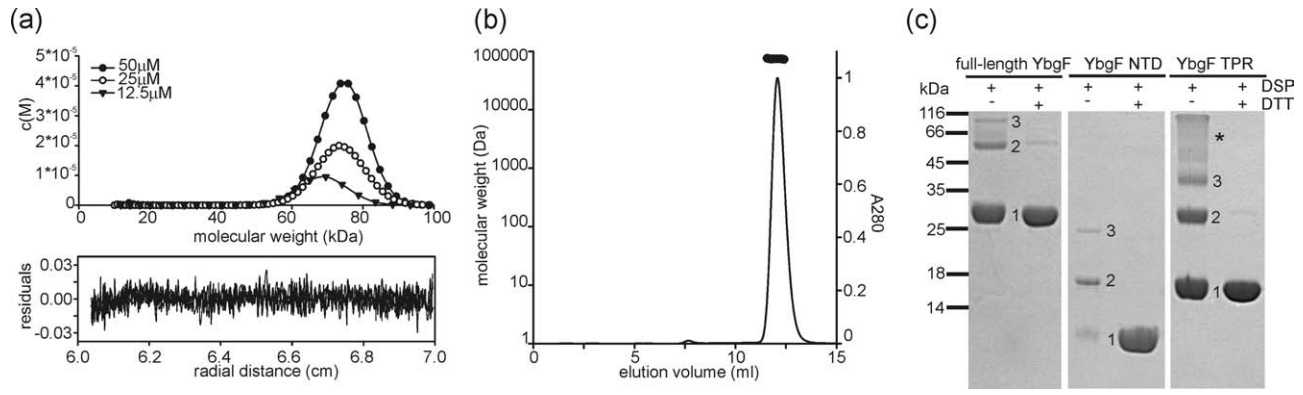

Figure 1

E. coli YbgF TPR domain self-associates in solution. (**a**) Analytical ultracentrifugation sedimentation velocity experiments on YbgF. c(M) distributions are shown for concentrations of 50 (●), 25 (○) and 12.5 μ*M* (▼) YbgF and the calculated molecular weight corresponds to that of a trimer at all three concentrations. Residuals of the fit for 50 μ*M* YbgF are shown on the bottom. (**b**) After SEC-MALLS, YbgF eluted as a single species with a molecular weight of 76.5 kDa (theoretical Mw for a trimer 76.2 kDa). (**c**) Intact YbgF, N-terminal domain (NTD) and TPR domain were cross-linked using DSP and separated by SDS-PAGE either with (+) or without (−) prior reduction of the cross-links with DTT. Bands corresponding to monomers (1), dimers (2) and trimers (3) as well as higher oligomers (*) for the TPR domain were visible after Coomassie staining.

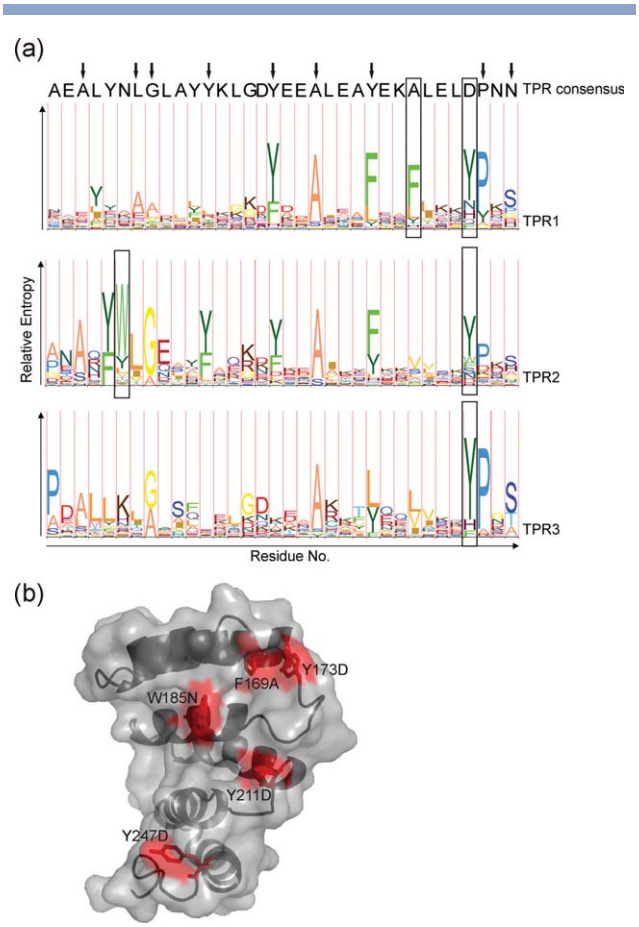

Figure 2

Identification of key residues in the oligomerization of the YbgF TPR domain. (**a**) HMM logos for the three consecutive TPR motifs in YbgF (labeled TPR1, 2, 3) are aligned with the TPR consensus sequence (top). Conserved residues that deviate from the consensus are indicated by boxes. Examples of conserved positions that are in agreement with the consensus are indicated by arrows. (**b**) Homology model for the YbgF TPR domain generated using the Geno3D server. The C-terminal capping helix could not be modeled. Residues indicated by boxes in (a) are shown as red sticks and red patches in the surface view. Residues Tyr173, Tyr211 and Tyr247 lie within loop regions separating the three TPR motifs, thus forming an exposed curved surface.

previously published TPR consensus[5] confirmed conservation of the key signature residues required for maintenance of the TPR fold in all three motifs [Fig. 2(a)]. Even beyond that, most other residues which are conserved among YbgF homologs match the TPR consensus, which argues for their involvement in stabilizing the TPR fold. Only five conserved positions were found that deviate from the TPR consensus [boxed residues in Fig. 2(a)]: A conserved Phe at position 27 in motif 1 (Ala in TPR consensus) and Trp at position 6 in motif 2 (Asn in TPR consensus) as well as conserved tyrosines at position 31 in all three motifs (Asp in TPR consensus). A homology model was generated for the TPR-domain of *E. coli* YbgF to evaluate the structural positioning of residues identified from the HMM logo [Fig. 2(b)]. Modeling was accomplished using the Geno3D server[37] and the three motif consensus protein CTPR3 structure as template (1na0.pdb,[5]), which has 24% sequence identity with the TPR-domain of YbgF. As evident from the model, the conserved Phe lies on the face of helix A in motif 1 that opposes helix B and is not ideally accessible for a potential binding partner, making it an unlikely candidate for a residue involved in binding. The Trp in motif 2 lies on the concave surface of the domain, which is known to form the ligand-binding surface in previously characterized TPR-complexes. The three conserved tyrosines lie in the loop regions separating consecutive TPR motifs and form an exposed surface for potential intermolecular interactions.

We mutated all five YbgF TPR residues to those of the TPR consensus and characterized the mutants' ability to form oligomers. However, proteins containing Phe-to-Ala or Trp-to-Asn mutations could not be expressed, suggesting a role for these residues in maintaining a stable fold rather than conferring binding specificity. Mutants containing Tyr-to-Asp mutations were successfully expressed and purified and the influence of individual tyrosines on trimerization and stability of the TPR domain was studied. We first followed the thermal denaturation of all four proteins by CD and as expected from their position in loop regions between adjacent motifs, none of the three tyrosine mutations perturbed the global fold of the TPR domain, with all mutants showing similar CD spectra to the wild type TPR at 20°C [Fig. 3(a)]. The wild type YbgF TPR domain showed a denaturation transition temperature (T_m) of 72°C, which was drastically decreased in all three engineered mutants. T_m was shifted by 10, 20, and 30°C compared to the wild type domain for YbgF TPR Y211D, Y173D, and Y247D, respectively [Fig. 3(b)].

We next carried out concentration-dependent cross-linking on the wild type and mutant YbgF TPR domains and found that oligomerization was significantly affected in two of the three mutants. Bands corresponding to dimeric, trimeric and higher oligomeric species were observed at concentrations as low as 1 μ*M* for the wild type domain and for the Y211D mutant, which also displayed the smallest change in thermal stability [Fig. 3(c)]. For Y173D, self-association was significantly weakened, with bands corresponding to oligomeric species only visible at concentrations of 30 and 10 μ*M*. For the Y247D mutant, the trimeric species was completely lost, while the dimer band remained visible at all concentrations used. Taken together, these experiments revealed that the YbgF TPR domain is more stable than other three-repeat TPR domains as a result of self-association; transition temperatures of 35–50°C have been reported for the monomeric three-repeat TPR domains of protein phosphatase 5 (PP5) and Hsp-organizing protein Hop.[38,39] Mutation of Tyr173, Tyr211 or Tyr247 to Asp,

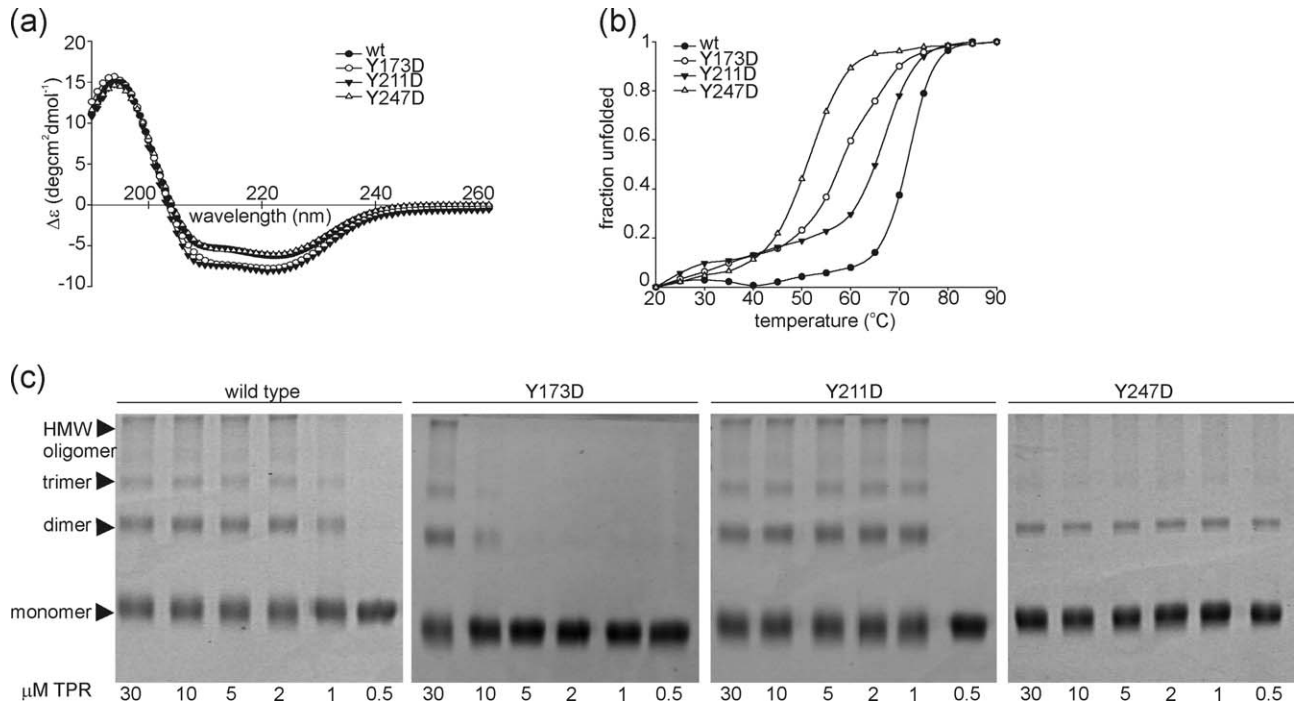

Figure 3

Stability and self-association of the YbgF TPR domain and Tyr-to-Asp mutants. (**a**) Wild type (●) TPR domain as well as mutants Y173D (○), Y211D (▼) and Y247D (Δ) all show similar CD spectra at 20°C. Analysis of spectra for secondary structure using CDNN software showed 75–80% α-helical content, the remainder random coil for all proteins. (**b**) Thermal denaturation experiments using wild type and mutant TPR domains. Transition midpoints of 72, 65, 58, and 51°C for wild type TPR, Y211D, Y173D, and Y247D, respectively, were recorded. (**c**) DSP cross-linking for wild type and mutant YbgF TPR domains at varying protein concentrations (0.5–30 μ*M*). Samples were run on nonreducing gels (in the absence of DTT) to preserve cross-links. Bands corresponding to monomers, dimers, trimers, and high molecular weight (HMW) oligomers are labeled.

which is the TPR consensus residue for this position, leads to destabilization of the TPR domain through weakening of intersubunit contacts. This results in a decrease of the melting temperature to 51–65°C for the mutants, which is within the expected range for monomeric TPR domains. We could therefore show that the three tyrosines identified from the HMM logo are key residues for oligomerization of the YbgF TPR domain, with the order of significance being Y173 > Y247 > Y211.

Engineering oligomerization into a consensus TPR domain

To test if the cumulative effect of the three tyrosine residues responsible for oligomerization of the YbgF TPR domain would be sufficient to induce self-association of TPR domains in general, we introduced them into a three-repeat consensus TPR protein, CTPR3. CTPR3 was obtained by probability-based consensus design and was previously reported to be monomeric based on its crystal-structure as well as solution data.[5] The triple Asp-to-Tyr mutant (CTPR3Y3) showed an almost identical CD spectrum to CTPR3, confirming that the mutations did not alter the overall TPR fold [Fig. 4(a)]. Chemical cross-linking and SEC-MALLS experiments comparing the oligomeric state of CTPR3 and CTPR3Y3 in solution confirmed that CTPR3 is monomeric. In contrast, CTPR3Y3 showed a cross-linking pattern very similar to that of YbgF TPR [Fig. 4(b)] and SEC-MALLS revealed the predominant species are higher oligomers, with a size distribution spanning 12- to 27-mers [Fig. 4(c)]. The propensity to oligomerize does not increase the overall stability of CTPR3Y3. Indeed, the mutant is destabilized significantly relative to CTPR3 (T_m decreased by ~30°C; data not shown). Hence, both decreasing TPR oligomerization (YbgF TPR domain; Fig. 3) or increasing TPR oligomerization (CTPR3Y3; Fig. 4) can result in reduced thermodynamic stability. In summary, our data show that the engineered TPR protein CTPR3Y3 forms higher order oligomers in solution consistent with our hypothesis that these residues contribute to oligomerization in TPR-containing proteins such as YbgF. This demonstrates that consensus-based design can be used to direct higher assembly structures for TPR proteins but that the stability of these folds is not readily predictable.

We next analyzed if the assembly of CTPR3Y3 into higher order oligomers could be modulated by the introduction of the YbgF N-terminal coiled-coil domain, as

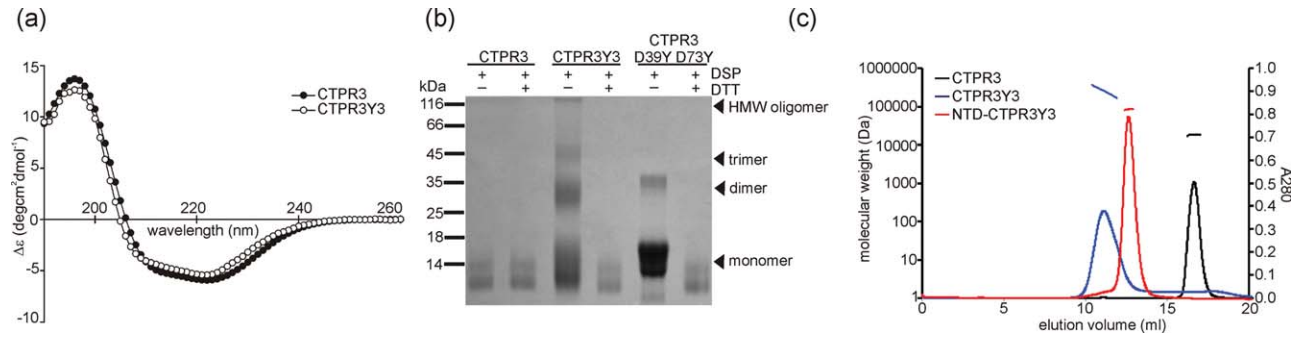

Figure 4

Engineering oligomerization into a monomeric consensus TPR protein. (**a**) CTPR3Y3 (○) and original CTPR3 (●) show similar CD spectra at 20°C in 10 m*M* sodium phosphate buffer pH 7.0, indicating preservation of the global fold in the mutant. Analysis of spectra for protein secondary structure content showed ~70% α-helical content for both proteins. (**b**) CTPR3, CTPR3Y3, and CTPR3 D39Y D73Y (where Tyr107 was mutated back to Asp) were cross-linked using DSP and separated by SDS-PAGE either with (+) or without (−) prior reduction of cross-links with DTT. While only monomer is seen for CTPR3, bands corresponding to monomer, dimer, trimer, and high molecular weight (HMW) oligomers are observed for CTPR3Y3. In contrast, the CTPR3 D39Y D73Y double mutant forms only dimers, similar to the YbgF TPR mutant Y247D [Fig. 3(c)]. (**c**) SEC-MALLS analysis of CTPR3 (black), CTPR3Y3 (blue) and the YbgF NTD-CTPR3Y3 fusion (red). CTPR3 is a single monomeric species (15 ± 0.5 kDa) while CTPR3Y3 is present as a mixture of higher order oligomers corresponding to 12–27 subunits. Fusion of CTPR3Y3 to the N-terminus of YbgF restricts its oligomeric state to a trimer (78 ± 2 kDa).

observed for YbgF. Fusing CTPR3Y3 to the YbgF NTD generated a fusion protein that only formed trimers in solution [Fig. 4(c)]. This proves that although the YbgF TPR domain has the potential to self-assemble into higher order structures, the protein's overall oligomeric state is restricted by the presence of its N-terminal coiled-coil domain.

Crystal structure of CTPR3 triple tyrosine mutant reveals a mode of assembly for higher order TPR oligomers

To characterize the role of the introduced tyrosine mutations at the interfaces of the engineered CTPR3Y3 mutant, we solved its crystal structure to a resolution of 2.2 Å by molecular replacement. Initially using the original CTPR3 structure (1na0.pdb) as a search model, the final solution was obtained using the coordinates of CTPR2 (1na3.pdb)[5] as template (see Table I for data-collection and refinement statistics). Electron density for an additional two residues (Pro5 and Gly6) could be resolved at the N-terminus of CTPR3Y3, compared to the original CTPR3 structure. Surprisingly, seventeen C-terminal residues, corresponding to the capping helix, were not resolved in the structure of CTPR3Y3. ESI-MS and SDS-PAGE of CTPR3Y3 crystals confirmed that the protein remains intact. Hence, the absence of electron density corresponding to the C-terminal capping helix is not due to proteolysis but a consequence of disorder. As described below, this disruption of the capping helix is linked to the ability of CTPR3Y3 to form stacked oligomers.

The structure of CTPR3Y3 shows that, with the exception of the capping helix, oligomerization does not cause any major changes to the TPR fold (see Fig. 5). Each subunit associates with two adjacent molecules by means of the engineered tyrosines [Fig. 6(a)]: Subunits 1 and 2 are oriented antiparallel, with the second subunit being related to the first by twofold symmetry along the *z*-axis, given by the symmetry operation $-y + 1, -x + 1, -z + 1/6$. The generated interface [denoted interface 1 in Fig. 6(a)] buries a surface area of 1411 Å^2 and involves Tyr39 and Tyr73 in the loop regions connecting TPR motifs 1/2 and 2/3, respectively, which stack against the same residues from the second subunit. The interface is further stabilized by eight hydrogen bonds, two of which involve Tyr39 (see Table II for a full list of pairwise residue contacts). The second interface [interface 2 in Fig. 6(a), buried surface area 1248 Å^2] is formed by tail-to-tail association of two adjacent subunits related by symmetry operation x, x−y+1,−z−1/6, with Tyr107 in subunit 2 contributing to this interface through a stacking interaction with its counterpart in subunit 3 [distance 4.1 Å, Fig. 6(b)]. The importance of this specific interface to self-association was shown by mutating Tyr107 back to Asp in the engineered oligomer CTPR3Y3, leaving D39Y and D73Y mutations intact, and analyzing the mutant by chemical cross-linking. The loss of Tyr107 from CTPR3Y3 resulted in a protein no longer able to trimerize but still able to form dimers [Fig. 4(b)], an effect identical to that of mutating the equivalent tyrosine (Tyr247) to Asp in the TPR domain of YbgF [Fig. 3(c)].

Analysis of the CTPR3Y3 structure using the EBI server PISA (Protein Interfaces, Surfaces and Assemblies)[40] suggests that interface 2 is significant in forming quaternary structure while interface 1 is not. Surface complementarity (Sc)[41] calculations however show that

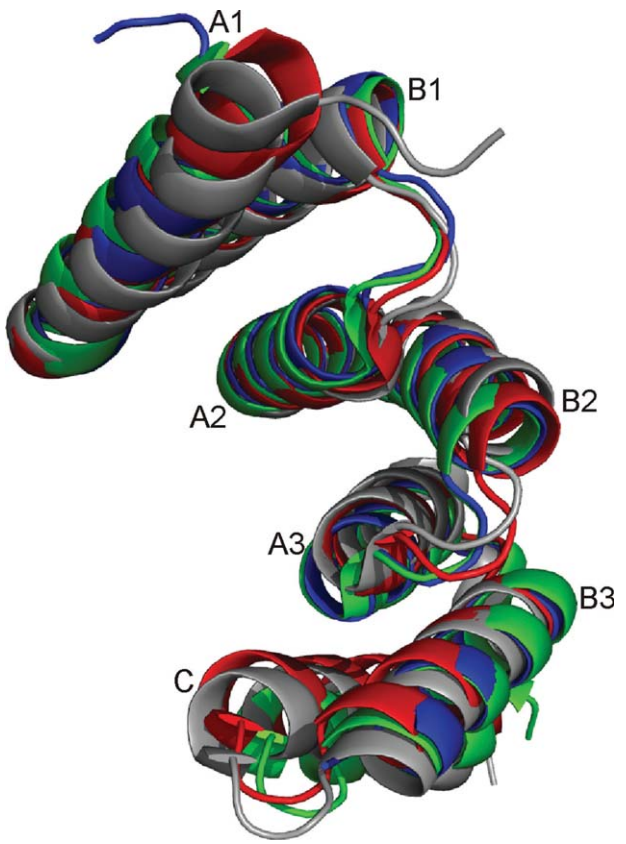

Figure 5

The TPR-fold remains unaltered in the engineered CTPR3Y3 oligomer. Overlay of CTPR3Y3 (blue, 2wqh.pdb), CTPR3 (green, 1na0.pdb), TPR domain of protein phosphatase 5 (gray, 2bug.pdb) and TPR domain of hSGT1 (red, 2vyi.pdb). Pairwise root mean square deviations (RMSD) are 0.56, 0.84, and 1.27 Å for CTPR3Y3 and CTPR3, hSGT1 or PP5, respectively. Helices A and B of motif 1–3 and the capping helix (C) are labeled.

both interfaces are typical of other protein–protein interactions. Interface 1 has an Sc index of 0.58, similar to that of antibody–antigen complexes, while interface 2 has an Sc of 0.81, which is typical of high affinity complexes and oligomeric proteins. These latter analyses are also consistent with the amino acid composition and interactions at each interface. Interface 2, predominantly made from the B3 helices of the contributing subunits, has a preponderance of hydrophobic amino acids (with few hydrogen bonds) while interface 1, composed of surface exposed loops of each subunit, is more polar and has a frequency of hydrogen bonds (one per 176 Å solvent accessible surface buried at the interface) typical of heteromeric protein complexes.[42]

The hydrogen bond that normally exists between Asp107 and the backbone amide of Asn109 is disrupted by the Asp107Tyr mutation in CTPR3Y3, resulting in increased flexibility of the loop region between TPR motif 3 and the capping helix. Strikingly, this causes the following proline (Pro108) to move by ~5 Å, displacing the capping helix from its position and disrupting its packing interactions with the last TPR motif [Fig. 7(a,b)]. These changes lead to unfolding of the capping helix, which is otherwise well resolved in the structure of monomeric CTPR3,[5] but absent in the CTPR3Y3 structure. Displacement of the capping helix further encourages the formation of alternative hydrophobic contacts between the B3 helices of subunits 2 and 3 [Fig. 7(a)]. These structural observations highlight a potential role for the capping helix in regulating TPR self-association. To test this idea, the capping helix (res. 111-125) was removed from the original CTPR3 protein and the resulting construct, CTPR3ΔC, tested for its ability to self-associate using DSP cross-linking [Fig. 7(c)]. While CTPR3

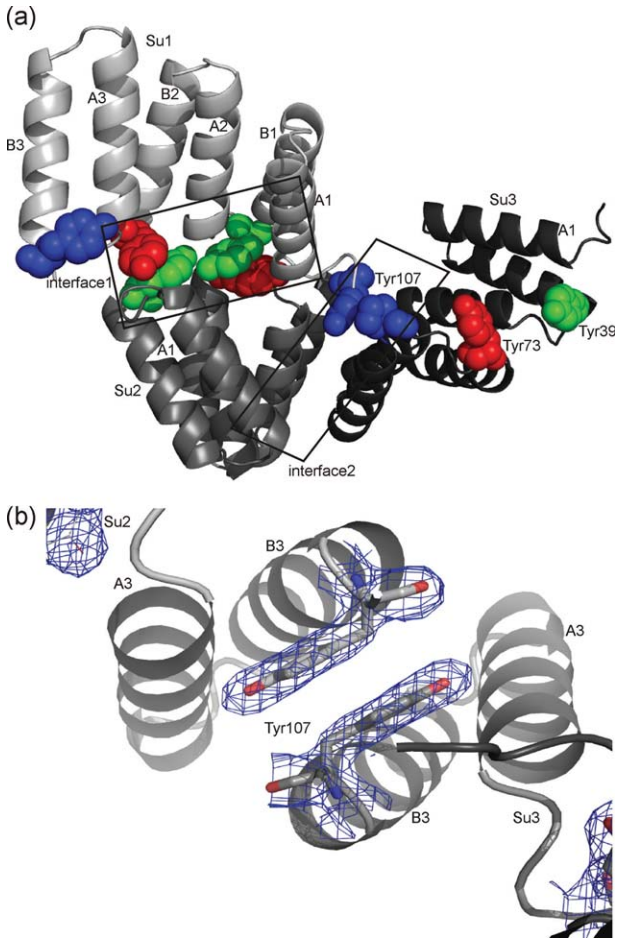

Figure 6

Structure of the asymmetric CTPR3Y3 trimer. (**a**) Three symmetry-related subunits (Su 1–3 shown in light, middle and dark gray, respectively) form an asymmetric trimer. Subunits 1 and 2 associate via Tyr39 (green, spacefill) and Tyr73 (red, spacefill), giving rise to interface 1. Tyr107 (blue, spacefill) is the key residue for interaction between subunits 2 and 3 (interface 2), leading to displacement of the capping helix which ordinarily packs against helix B3 in the CTPR3 structure. (**b**) Electron density for Tyr107 from subunits 2 and 3.

Table II
List of Pairwise Contacts Contributing to Interface 1 and 2 of the CTPR3Y3 Trimer

Interface 1			
Hydrogen bonds			
No.	Subunit 1	Subunit 2	Distance (Å)
1	Tyr 13 [OH]	Glu 10 [OE1]	2.71
2	Asn 41 [ND2]	Leu 72 [O]	2.94
3	Ala 43 [N]	Tyr 39 [OH]	3.13
4	Asn 75 [ND2]	Leu 38 [O]	3.38
5	Glu 10 [OE1]	Tyr 13 [OH]	2.71
6	Leu 72 [O]	Asn 41 [ND2]	2.94
7	Tyr 39 [OH]	Ala 43 [N]	3.13
8	Leu 38 [O]	Asn 75 [ND2]	3.38
Stacking			
9	Tyr 39	Tyr 73	4.07–4.98
10	Tyr 73	Tyr 39	4.07–4.98
Interface 2			
Hydrogen bonds			
No.	Subunit 2	Subunit 3	Distance (Å)
1	Gln 101 [NE2]	Tyr 100 [OH]	2.96
2	Tyr 100 [OH]	Gln 101 [NE2]	2.96
Stacking			
3	Tyr 107	Tyr 107	4.05–4.26

Numbering considers Gly in the sequence of the TEV-cleaved protein as residue 1.

did not form oligomers, even when a 50-fold excess of cross-linker was used, CTPR3ΔC readily formed oligomers. However, these associations are weak since analysis of CTPR3ΔC by SEC-MALLS indicated that only the monomeric state was stable in solution (data not shown). These data show that displacement of the capping helix drives subunit association but that further stabilizing forces, such as the hydrogen bonds and stacking interactions emanating from the engineered tyrosines in CTPR3Y3, are required to increase the stability of the resulting oligomers.

The two different interfaces formed between subunits 1 and 2 and 2 and 3, respectively, give rise to a quasi-continuous oligomeric TPR stack of asymmetric TPR trimers as building blocks, which form a fiber-like superstructure that runs throughout the crystal [Fig. 8(a)]. Although elongated oligomers consisting of 12-27 subunits were observed in solution [Fig. 4(c)], we did not observe fibers. This could be due to the lower concentrations used in solution experiments (up to 200 μ*M*) relative to crystallization conditions (690 μ*M*). Previous work has shown that proteins consisting of multiple TPRs arranged in tandem, where adjacent helices pack against each other in an antiparallel way, form a right-handed superhelix with a diameter of ~40 Å and a pitch of ~70 Å [Fig. 8(b)[6,21]]. In contrast, CTPR3Y3 does not form a regular superhelix; the parallel packing of helix 6 from two adjacent subunits causes the local unwinding of the otherwise superhelical structure, which has a pitch of ~120 Å, corresponding to the length of the unit cell *c*-axis, and a width of ~60 Å. This shows that the noncovalent assembly of multiple TPR motifs allows for greater structural variability than can be achieved by covalent tandem arrays of the same repeat unit.

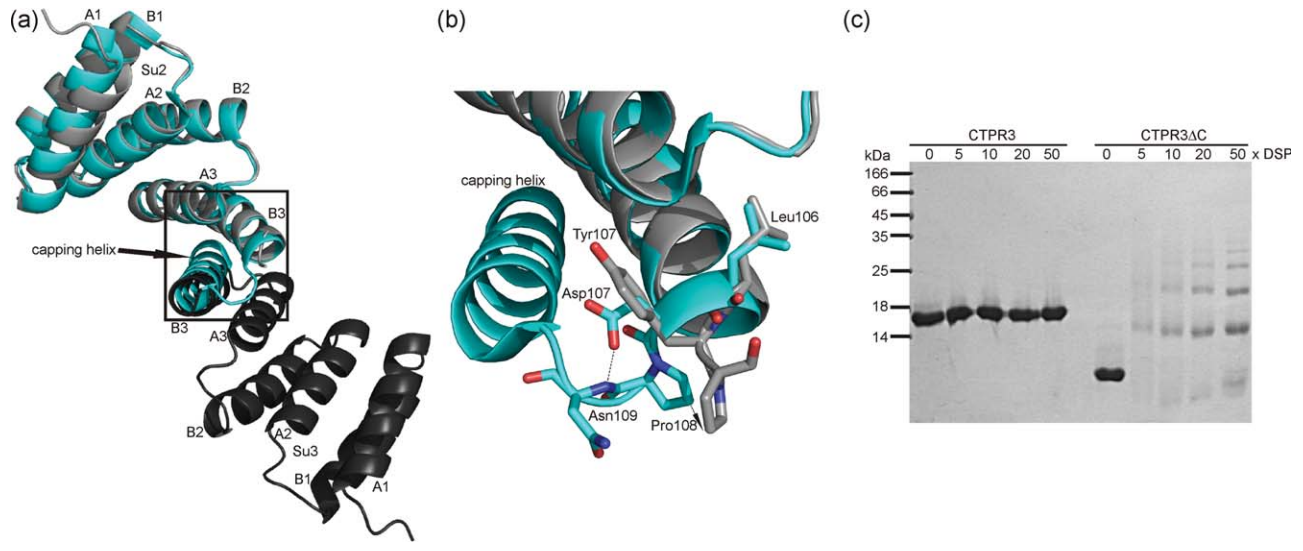

Figure 7
(**a**) Overlay of two interacting CTPR3Y3 subunits (Su2 light gray, Su3 dark gray) with the original CTPR3 structure (cyan). Formation of interface 2 in the CTPR3Y3 trimer involves the B-helices of two adjacent subunits and helix B3 from Su3 displacing the capping helix of Su2. (**b**) In CTPR3, Asp107 forms a hydrogen bond with the backbone amide of Asn109 (distance 3.1 Å), stabilizing the loop between TPR motif 3 and locking the capping helix in its position packed against helix B3. In CTPR3Y3, the stabilizing hydrogen bond is lost through a D107Y mutation, causing increased flexibility of the loop and capping helix. This is reflected by a conformational change of Pro108 (indicated by the arrow), changing the directionality of the chain and moving the capping helix away from the B-helix. (**c**) Displacement of the capping helix drives self-association. DSP cross-linking was carried out on CTPR3 and CTPR3ΔC showing that CTPR3ΔC self-associates in a similar fashion to CTPR3Y3.

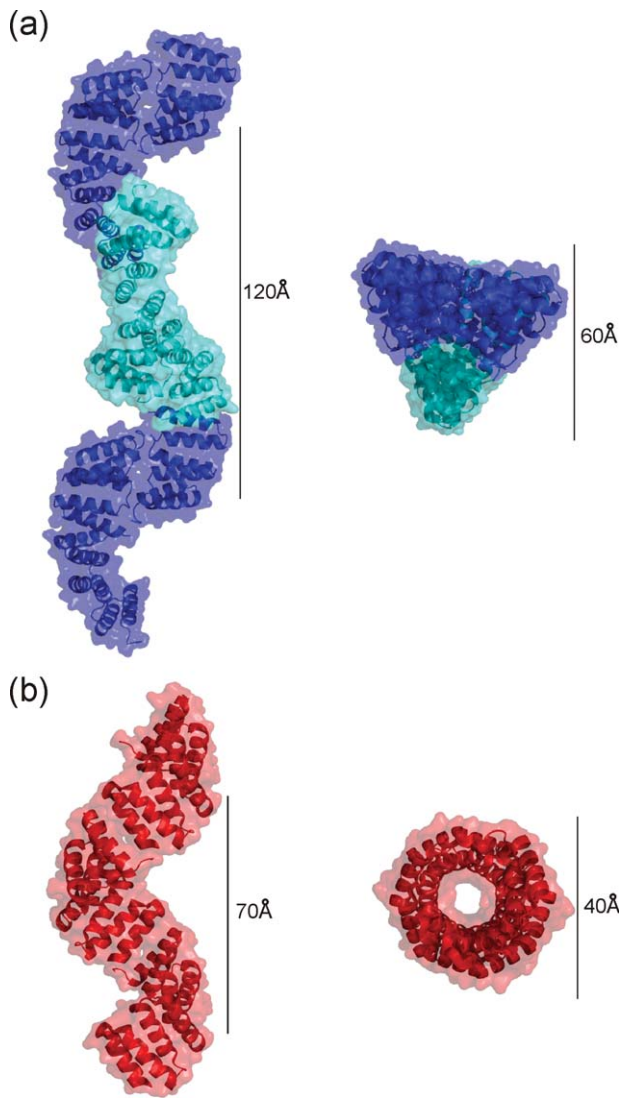

Figure 8

Structural comparison of CTPR8 and CTPR3Y3. (**a**) Noncovalently assembled CTPR3Y3 trimers (light and dark blue) form an extended twisted stack with a pitch of ~120 Å and a diameter of ~60 Å. The right-handed twist is interrupted by the parallel packing of two TPR motifs at interface 2, which leads to unwinding of the superhelix. (**b**) Multiple covalently linked tandem repeats of TPR motifs give rise to a right-handed superhelical structure with a pitch of ~70 Å and a diameter of ~40 Å in the case of CTPR8 (2hyz.pdb).[21]

DISCUSSION

Engineered oligomerization of a consensus TPR domain as means of understanding YbgF self-association

In all structurally characterized TPR-ligand complexes studied to date the TPR-domain does not undergo any major conformational changes upon ligand-binding.[8–11] This, together with the invariability of motif length, makes them attractive targets for engineering novel binding specificities. We identified residues important for oligomerization of TPRs by subtracting TPR signature residues from residues conserved within a certain group of oligomeric TPR proteins (YbgF homologs). A similar approach has been used previously to highlight residues potentially mediating binding specificity,[33] but was used here to direct the formation of homo-oligomers. A striking consequence of the three Asp-to-Tyr mutation-induced oligomerization of CTPR3Y3 is the formation of an asymmetric trimer. The two distinct interfaces of the trimer, head-to-tail at interface 1 and tail-to-tail at interface 2, lead to the formation of a noncovalent TPR stack stabilized by the introduced tyrosine residues that has different superhelical dimensions to that of multiple covalently linked TPR motifs. Asymmetric protein trimers have been reported previously,[43–45] but these do not result in a stacked arrangement of oligomers because similar or related interfaces are involved in forming the assembly.

Structural analysis on TPR domains deposited in the Protein Data Bank using PISA[40] reveals the possibility of self-association in a number of cases. For example, PilF (2fi7.pdb), a component of the *Pseudomonas aeruginosa* type 4 pilus biogenesis system[46] and the TPR domain of the putative FK506-binding protein PFL2275c from *Plasmodium falciparum* (2fbn.pdb[47]) both form crystallographic dimers. However, there is no solution data confirming the interfaces involved in self-association are biologically relevant. In addition, no structural information on higher order TPR oligomers, like those formed by Fis1, rapsyn or AtTDX,[13,15,16] is currently available. In the case of Fis1, structural data even contradicts the available solution data. Although the formation of biologically relevant, higher order oligomers was clearly demonstrated by Serasinghe and Yoon,[16] the crystal structure of hFis1 TPR-domain (1nzn.pdb) shows Fis dimers formed via interfaces that conflict with the mutagenesis data. Thus, the structure of CTPR3Y3 presented here for the first time allows detailed insight into the possible mode of assembly for higher order TPR-mediated structures where both structural and solution data are in agreement.

We have as yet been unable to determine the crystal structure of the *E. coli* YbgF TPR domain for direct comparison to the solution data reported here. It is therefore pertinent to ask how relevant the crystal structure of CTP3Y3 is for explaining the oligomerization behavior of the YbgF TPR domain? Four observations collectively indicate that their modes of self-assembly must be similar if not identical: First, the monomeric consensus TPR protein CTPR could be made to oligomerize into trimeric structures simply by substituting aspartic acid residues in interhelical loop regions with tyrosines, as found in most bacterial YbgF homologues. Second, the pattern of tyrosine interactions observed in the CTPR3Y3 crystal structure readily explains the cross-linking data for YbgF

TPR mutants. Mutation of Tyr247 in the YbgF TPR domain, equivalent to Tyr107 in CTPR3Y3, leads to formation of a dimeric instead of a trimeric form [Fig. 3(c)], with an identical effect observed for the equivalent CTPR3Y3 mutant [Fig. 4(b)]. Tyr107 is essential to the stability of interface 2 in the CTPR3Y3 trimer [Fig. 6(a)], its loss expected to yield a dimeric species. Moreover, the loss of interface 2 and hence the asymmetry of the trimer would abolish the ability of the TPR domain to form higher order (>3 subunits) oligomeric states, which is again what is observed when Tyr247/Tyr107 are mutated. Mutation of YbgF TPR Tyr173 (equivalent to Tyr39 in CTPR3Y3) has a more severe effect on oligomerization than Tyr211 (equivalent to Tyr73 in CTPR3Y3) [Fig. 3(c)]. Although both tyrosines are involved in stabilizing interface 1 in CTPR3Y3 [Fig. 6(a)] Tyr39 forms additional hydrogen bonds to the backbone of the opposing subunit, explaining its greater importance to self-association and hence its greater impact when mutated. Third, the asymmetry of the CTPR3Y3 trimer explains how the protein is able to form higher order aggregates [observed in the crystal, Fig. 8(a), and by SEC-MALLS experiments; Fig. 4(c)] and so provides an explanation as to how the YbgF TPR trimer can similarly form higher order oligomeric states, albeit ones that are less stable and only observable by cross-linking [Fig. 1(c)]. Fourth, the N-terminal trimeric coiled-coil domain of intact YbgF restricts the ability of both the YbgF TPR domain and CTPR3Y3 to form these higher order oligomeric structures, emphasizing the similarity in their mechanisms of self-association and how these can be moderated by additional domains.

Rules for the self-association of TPRs and the role of the capping helix

Since the structure presented here is to our knowledge the first example of a higher order oligomer formed between TPR-domains and, most importantly, was confirmed to be identical to the oligomers formed in solution, it goes some way in answering if different interfaces are involved in ligand-binding as opposed to self-association. While ligands usually bind to the concave surface of TPR arrays, we observed two distinct classes of interfaces in the case of homo-oligomerization, none of which involved the TPR inner groove. Interface 1 is formed across the loop regions connecting adjacent TPR motifs through stacking interactions between the engineered tyrosines. Interface 2 mimics helix–helix associations which usually occur between adjacent tandem TPRs, with the difference that in this case of noncovalent assembly the two interacting helices associate in parallel. Formation of this interface replaces the capping helix, which is otherwise packed against the B-helix of the last TPR motif in an antiparallel fashion (see Fig. 7). A similar phenomenon has been observed with larger TPR tandem arrays like CTPR8 and CTPR20.[21] Although these are monomeric in solution, the capping helix is displaced in the crystal to facilitate lattice contacts, leading to a "hypersymmetric" superhelical structure.

The structure of CTPR3Y3 shows that TPR oligomerization in solution takes place via a similar mechanism, with the difference that displacement of the capping helix is facilitated by the introduction of a tyrosine mutation which both compromises tethering of the loop between the last TPR motif and the capping helix and actively engages in an interaction stabilizing the alternative interface between two adjacent subunits (see Fig. 7). For this to happen, the energy barrier for displacement of the capping helix must be relatively low, a likely consequence of its more hydrophilic nature compared to internal TPR helices. It is conceivable that capping helix displacement by competing interactions between TPR subunits is an oligomerization mechanism of general applicability. The protein Sgt1, for example, which acts as a regulator of the innate immune response in plants and is required for kinetochore assembly in yeast,[19,48–50] has been found to dimerize by virtue of its three-repeat TPR domain.[17,19] In the case of Barley Sgt1, this depends on the redox state of the protein: Under oxidizing conditions a disulfide bridge forms between the helix A3 and the capping helix which inhibits dimerization.[17] Although no structural information is available on the Sgt1 dimer to elucidate the mechanism behind this case of redox-dependent self-association, we propose that it might involve oligomerization-dependent displacement of the capping helix. This would explain why under oxidizing conditions, where packing of the capping helix is stabilized by a disulfide bond, self-association is inhibited. In the case of Fis1, it has been shown that the hydrophilic N-terminal helix (α1), which seems to act as capping helix, has an inhibitory effect on oligomerization of the TPR-domain.[12] Moreover, two well conserved tyrosines can be found in the loop regions between α2/3 and α4/5 of the two TPR motifs in Fis1 which, despite being located on the opposite face of the TPR domain, could form a similar interface as observed in CTPR3Y3. Indeed, Zhang *et al.*[12] presented solution data showing Tyr87 plays a crucial role in Fis1 oligomerization. The two cases presented above demonstrate that the mechanisms leading to oligomerization of CTPR3Y3 are likely to be of general applicability for the self-association of TPR-containing proteins.

TPR-oligomerization gives rise to new binding surfaces

Self-association extends the repertoire of possible higher order structures generated by TPRs from the regular right-handed superhelix seen in TPR tandem arrays to a locally unwound or twisted helix as observed in the CTPR3Y3 structure (see Fig. 8). In the case of rapsyn it

has been shown that TPR-dependent clustering of the protein is a prerequisite for binding and clustering of acetylcholine receptors.[13,14] Similarly, for yeast Sgt1, dimerization via the TPR domain is necessary for and precedes the recruitment of both Skp1 and Hsp90, which is necessary for assembly of the kinetochore complex CBF3.[19] It is conceivable that the distinct surfaces generated by self-assembly of TPRs give rise to new ligand binding sites therefore creating a further level of organization centered on TPR-containing protein complexes.

ACKNOWLEDGMENTS

The authors are grateful to Lynne Regan (Yale University) for providing the expression construct for CTPR3, and Andrew Leech and Berni Strongitharm (York Technology Facility) for help with analytical ultracentrifugation and ESI-MS experiments. They thank Johan Turkenburg, Sam Hart, and Eleanor Dodson (York Structural Biology Laboratory) for help with data collection and crystallographic discussions.

REFERENCES

1. Hirano T, Kinoshita N, Morikawa K, Yanagida M. Snap helix with knob and hole: essential repeats in *S. pombe* nuclear protein nuc2+. Cell 1990;60:319–328.
2. Sikorski RS, Boguski MS, Goebl M, Hieter P. A repeating amino acid motif in CDC23 defines a family of proteins and a new relationship among genes required for mitosis and RNA synthesis. Cell 1990;60:307–317.
3. Goebl M, Yanagida M. The TPR snap helix: a novel protein repeat motif from mitosis to transcription. Trends Biochem Sci 1991;16: 173–177.
4. Main ER, Jackson SE, Regan L. The folding and design of repeat proteins: reaching a consensus. Curr Opin Struct Biol 2003;13:482–489.
5. Main ER, Xiong Y, Cocco MJ, D'Andrea L, Regan L. Design of stable alpha-helical arrays from an idealized TPR motif. Structure 2003;11:497–508.
6. Das AK, Cohen PW, Barford D. The structure of the tetratricopeptide repeats of protein phosphatase 5: implications for TPR-mediated protein–protein interactions. EMBO J 1998;17:1192–1199.
7. D'Andrea LD, Regan L. TPR proteins: the versatile helix. Trends Biochem Sci 2003;28:655–662.
8. Abe Y, Shodai T, Muto T, Mihara K, Torii H, Nishikawa S, Endo T, Kohda D. Structural basis of presequence recognition by the mitochondrial protein import receptor Tom20. Cell 2000;100:551–560.
9. Cliff MJ, Harris R, Barford D, Ladbury JE, Williams MA. Conformational diversity in the TPR domain-mediated interaction of protein phosphatase 5 with Hsp90. Structure 2006;14:415–426.
10. Gatto GJ Jr, Geisbrecht BV, Gould SJ, Berg JM. Peroxisomal targeting signal-1 recognition by the TPR domains of human PEX5. Nat Struct Biol 2000;7:1091–1095.
11. Scheufler C, Brinker A, Bourenkov G, Pegoraro S, Moroder L, Bartunik H, Hartl FU, Moarefi I. Structure of TPR domain-peptide complexes: critical elements in the assembly of the Hsp70-Hsp90 multichaperone machine. Cell 2000;101:199–210.
12. Zhang Y, Chan DC. Structural basis for recruitment of mitochondrial fission complexes by Fis1. Proc Natl Acad Sci USA 2007;104: 18526–18530.
13. Ramarao MK, Bianchetta MJ, Lanken J, Cohen JB. Role of rapsyn tetratricopeptide repeat and coiled-coil domains in self-association and nicotinic acetylcholine receptor clustering. J Biol Chem 2001;276:7475–7483.
14. Eckler SA, Kuehn R, Gautam M. Deletion of N-terminal rapsyn domains disrupts clustering and has dominant negative effects on clustering of full-length rapsyn. Neuroscience 2005;131:661–670.
15. Lee JR, Lee SS, Jang HH, Lee YM, Park JH, Park SC, Moon JC, Park SK, Kim SY, Lee SY, Chae HB, Jung YJ, Kim WY, Shin MR, Cheong GW, Kim MG, Kang KR, Lee KO, Yun DJ, Lee SY. Heat-shock dependent oligomeric status alters the function of a plant-specific thioredoxin-like protein, AtTDX. Proc Natl Acad Sci USA 2009;106:5978–5983.
16. Serasinghe MN, Yoon Y. The mitochondrial outer membrane protein hFis1 regulates mitochondrial morphology and fission through self-interaction. Exp Cell Res 2008;314:3494–3507.
17. Nyarko A, Mosbahi K, Rowe AJ, Leech A, Boter M, Shirasu K, Kleanthous C. TPR-Mediated self-association of plant SGT1. Biochemistry 2007;46:11331–11341.
18. Bansal PK, Mishra A, High AA, Abdulle R, Kitagawa K. Sgt1 dimerization is negatively regulated by protein kinase CK2-mediated phosphorylation at Ser361. J Biol Chem 2009;284:18692–18698.
19. Bansal PK, Nourse A, Abdulle R, Kitagawa K. Sgt1 dimerization is required for yeast kinetochore assembly. J Biol Chem 2009;284: 3586–3592.
20. Cortajarena AL, Kajander T, Pan W, Cocco MJ, Regan L. Protein design to understand peptide ligand recognition by tetratricopeptide repeat proteins. Protein Eng Des Sel 2004;17:399–409.
21. Kajander T, Cortajarena AL, Mochrie S, Regan L. Structure and stability of designed TPR protein superhelices: unusual crystal packing and implications for natural TPR proteins. Acta Crystallogr D Biol Crystallogr 2007;63(Part 7):800–811.
22. Bohm G, Muhr R, Jaenicke R. Quantitative analysis of protein far UV circular dichroism spectra by neural networks. Protein Eng 1992;5:191–195.
23. Schuck P. Size-distribution analysis of macromolecules by sedimentation velocity ultracentrifugation and lamm equation modeling. Biophys J 2000;78:1606–1619.
24. Otwinowski Z, Borek D, Majewski W, Minor W. Multiparametric scaling of diffraction intensities. Acta Crystallogr A 2003;59(Part 3):228–234.
25. Emsley P, Cowtan K. Coot: model-building tools for molecular graphics. Acta Crystallogr D Biol Crystallogr 2004;60(Part 12 Part 1): 2126–2132.
26. Murshudov GN, Vagin AA, Dodson EJ. Refinement of macromolecular structures by the maximum-likelihood method. Acta Crystallogr D Biol Crystallogr 1997;53(Part 3):240–255.
27. Davis IW, Leaver-Fay A, Chen VB, Block JN, Kapral GJ, Wang X, Murray LW, Arendall WB III, Snoeyink J, Richardson JS, Richardson DC. MolProbity: all-atom contacts and structure validation for proteins and nucleic acids. Nucleic Acids Res 2007;35(Web Server issue):W375–W383.
28. Schultz J, Milpetz F, Bork P, Ponting CP. SMART, a simple modular architecture research tool: identification of signaling domains. Proc Natl Acad Sci USA 1998;95:5857–5864.
29. Lazzaroni JC, Portalier RC. Genetic and biochemical characterization of periplasmic-leaky mutants of Escherichia coli K-12. J Bacteriol 1981;145:1351–1358.
30. Levengood-Freyermuth SK, Click EM, Webster RE. Role of the carboxyl-terminal domain of TolA in protein import and integrity of the outer membrane. J Bacteriol 1993;175:222–228.
31. Lubkowski J, Hennecke F, Pluckthun A, Wlodawer A. Filamentous phage infection: crystal structure of g3p in complex with its coreceptor, the C-terminal domain of TolA. Structure 1999;7:711–722.
32. Cascales E, Buchanan SK, Duche D, Kleanthous C, Lloubes R, Postle K, Riley M, Slatin S, Cavard D. Colicin biology. Microbiol Mol Biol Rev 2007;71:158–229.
33. Blatch GL, Lassle M. The tetratricopeptide repeat: a structural motif mediating protein–protein interactions. Bioessays 1999;21:932–939.

34. Larkin MA, Blackshields G, Brown NP, Chenna R, McGettigan PA, McWilliam H, Valentin F, Wallace IM, Wilm A, Lopez R, Thompson JD, Gibson TJ, Higgins DG. Clustal W and Clustal X version 2.0. Bioinformatics 2007;23:2947–2948.
35. Schuster-Bockler B, Schultz J, Rahmann S. HMM Logos for visualization of protein families. BMC Bioinformatics 2004;5:7.
36. Pagni M, Ioannidis V, Cerutti L, Zahn-Zabal M, Jongeneel CV, Hau J, Martin O, Kuznetsov D, Falquet L. MyHits: improvements to an interactive resource for analyzing protein sequences. Nucleic Acids Res 2007;35(Web Server issue):W433–W437.
37. Combet C, Jambon M, Deleage G, Geourjon C. Geno3D: automatic comparative molecular modelling of protein. Bioinformatics 2002; 18:213–214.
38. Cliff MJ, Williams MA, Brooke-Smith J, Barford D, Ladbury JE. Molecular recognition via coupled folding and binding in a TPR domain. J Mol Biol 2005;346:717–732.
39. Cortajarena AL, Regan L. Ligand binding by TPR domains. Protein Sci 2006;15:1193–1198.
40. Krissinel E, Henrick K. Inference of macromolecular assemblies from crystalline state. J Mol Biol 2007;372:774–797.
41. Lawrence MC, Colman PM. Shape complementarity at protein/protein interfaces. J Mol Biol 1993;234:946–950.
42. Lo Conte L, Chothia C, Janin J. The atomic structure of protein–protein recognition sites. J Mol Biol 1999;285:2177–2198.
43. Liao DI, Wawrzak Z, Calabrese JC, Viitanen PV, Jordan DB. Crystal structure of riboflavin synthase. Structure 2001;9:399–408.
44. Seeger MA, Schiefner A, Eicher T, Verrey F, Diederichs K, Pos KM. Structural asymmetry of AcrB trimer suggests a peristaltic pump mechanism. Science 2006;313:1295–1298.
45. Shimomura Y, Wada K, Fukuyama K, Takahashi Y. The asymmetric trimeric architecture of [2Fe-2S] IscU: Implications for its scaffolding iron-sulfu cluster biosynthesis. J Mol Biol 2008;383:133–143.
46. Kim K, Oh J, Han D, Kim EE, Lee B, Kim Y. Crystal structure of PilF: functional implication in the type 4 pilus biogenesis in *Pseudomonas aeruginosa.* Biochem Biophys Res Commun 2006;340: 1028–1038.
47. Vedadi M, Lew J, Artz J, Amani M, Zhao Y, Dong A, Wasney GA, Gao M, Hills T, Brokx S, Qiu W, Sharma S, Diassiti A, Alam Z, Melone M, Mulichak A, Wernimont A, Bray J, Loppnau P, Plotnikova O, Newberry K, Sundararajan E, Houston S, Walker J, Tempel W, Bochkarev A, Kozieradzki I, Edwards A, Arrowsmith C, Roos D, Kain K, Hui R. Genome-scale protein expression and structural biology of *Plasmodium falciparum* and related Apicomplexan organisms. Mol Biochem Parasitol 2007;151:100–110.
48. Azevedo C, Sadanandom A, Kitagawa K, Freialdenhoven A, Shirasu K, Schulze-Lefert P. The RAR1 interactor SGT1, an essential component of R gene-triggered disease resistance. Science 2002;295: 2073–2076.
49. Liu Y, Schiff M, Serino G, Deng XW, Dinesh-Kumar SP. Role of SCF ubiquitin-ligase and the COP9 signalosome in the N gene-mediated resistance response to Tobacco mosaic virus. Plant Cell 2002;14:1483–1496.
50. Peart JR, Lu R, Sadanandom A, Malcuit I, Moffett P, Brice DC, Schauser L, Jaggard DA, Xiao S, Coleman MJ, Dow M, Jones JD, Shirasu K, Baulcombe DC. Ubiquitin ligase-associated protein SGT1 is required for host and nonhost disease resistance in plants. Proc Natl Acad Sci USA 2002;99:10865–10869.